JOURNAL OF GEOPHYSICAL RESEARCH, VOL. ???, NO. , PAGES 1–36,

Weddell sea-iceberg drift: 5 years of observations

M. P. Schodlok,[1] H. H. Hellmer,[1] G. Rohardt,[1] and E. Fahrbach[1]

M. P. Schodlok, Alfred Wegener Institute for Polar and Marine Research, Bremerhaven, Germany. (mschodlok@awi-bremerhaven.de)

[1]Alfred Wegener Institute for Polar and Marine Research, Bremerhaven, Germany

Abstract.

The drift of 52 icebergs tagged with GPS buoys in the Weddell Sea since 1999 has been investigated with respect to prevalent drift tracks, sea-ice/icberg interaction and freshwater fluxes. Buoys were deployed on small to medium sized icebergs (edge sizes $\leq$ 5 km) in the south-western and eastern Weddell Sea. With this buoy distribution the basin scale iceberg drift of this size class was established. In the western Weddell Sea icebergs followed a northward course with little deviations with mean daily drift rates of xxxxx m/s. The observed iceberg drift to the west of 40°W showed coherent motions with the sea ice. In the highly consolidated prennial sea-ice cover of 95 % the sea ice has a steering influence on the icebergs and is thus reponsible for the coherent drift tracks. The northward drift of buoys to the east of 40°W is interrupted with large deviations due to passages of low pressure systems. Mean speads in this area were xxxx m/s. Examining the sea-ice concentration with AMSR-E satellite data resulted in a value of 86 % for a coherent sea-ice iceberg movement. The length scale of coherent movement was estimated to be less than 250 km; about half the value found for the Arctic Ocean. The freshwater fluxes estimated from three iceberg export scenarios deduced from the iceberg drift pattern were highly variable. Assuming a residence time in the Weddell Sea of one year the icebergs melt water input is 31 Gt if all iceberg calved are exported. This is about a third of the basal melt water input from Filchner Ronne Ice Shelf.

1. Introduction

"As the day wore on the bergs, instead of diminishing in number, actually increased: and wonder we had felt in the morning increased to amazement. Every mile forward brought new columns into sight. They seemed inexhaustible. A grander display of ice-power had perhaps never been seen. In a twenty-four hour period ending December 28^{th} Dr. Poulter estimated we sighted 8000 bergs." [*Byrd*, 1935, p. 51]. This account from the 2^{nd} Byrd Antarctic Expedition (1933–1935), near 66°S, 139.5°W, approximately 2000 km north of Marie Byrd Land, illustrates the massive loss to the Antarctic ice sheet due to continuous calving. While sightings on such a scale are rare they raise questions as to the potential of iceberg impact on hydrology, circulation and biology which are related to drift and melting.

The mean annual iceberg calving rate in the Southern Hemisphere is estimated to be 2016 Gt/a [Jacobs *et al.*, 1992]. This value is associated with uncertainties in size assessment, i.e., volume estimate, event frequency and decay rate between calving and observation. Assuming a mean iceberg density of 850 kg m^{-3} [Weeks and Mellor, 1978], the calving rate represents an equivalent volume of 75.21 mSv (1 mSv = 10^3 m^3s^{-1}) of freshwater which is transferred to the upper Southern Ocean water column. This is approximately 20% of the annual National Centers for Environmental Prediction (NCEP) net precipitation (P-E) value (413 mSv) into the Southern Ocean south of 55°S and is far larger than the freshwater flux due to ice shelf basal melting (28 mSv) [Hellmer, 2004].

The implications of iceberg melt water for the Southern Ocean hydrography and marine biology depend upon the location and quantity of melting. Numerical studies of the impact of ice shelf basal melt water showed that the weakly stratified continental shelf

water column is sensitive to changes in the freshwater fluxes: an addition stabilizes the water column and decreases dense water formation, while a reduction enhances deep convection and leads to sea-ice thinning [Hellmer, 2004]. The role of iceberg melt water in this freshwater balance is not well known.

In addition, iceberg melt water contains meteoric dust (up to 1.4 10^{-6} kg per 1 m^3 of ice; Wagenbach, pers. comm. 2003), accumulated on the ice sheet over several thousands of years. Micro-nutrients within the dust, such as iron, may contribute to the fertilization of the upper ocean when released by melting. Melt-driven upwelling in the vicinity of icebergs may have a similar effect as it can bring nutrient-rich deeper waters to the euphotic zone.

Iceberg groundings cause long-term disturbances to the local benthic ecosystem [Gutt and Starmans, 2001] and to hydrographic conditions [Nøst and Østerhus, 1998]. With a decrease in temperature and salinity the community composition can shift in favour of those species which can adapt most rapidly to the new conditions in the nearby water column. In 1986, the giant icebergs A22, A23, and A24 stranded on the shallow Berkner Bank (42°W, 76°S). This grounding altered the sea-ice coverage, water mass characteristics, and the flow pattern in the Filchner Trough [Grosfeld *et al.*, 2001]. Despite the potentially far-reaching impacts of iceberg melting little is known about prevelant berg drift tracks, i.e. the location and quantity of freshwater input in the Weddell Sea.

Technology for monitoring drift tracks has advanced considerably over the last 30 years. Giant tabular iceberg with edges longer than 18.5 km (satellite sensor detection limit is 10 nm (1 nm = 1.852 km)) calving along the Antarctic continental coastline have been monitored by active and passive satellite remote sensing since the late 1970's by, for example, the National Ice Center (NIC). The early observations by, e.g., Swithinbank *et al.* [1977]

established that the main northward drift routes in the western Ross and Weddell seas lead icebergs away from the major ice shelves towards and into the Antarctic Circumpolar Current. However, massive calving events, such as the most recent of Filchner-Ronne (1998/99) and Ross ice shelves (2001/02), occur infrequently. Melting and break up to sizes below the detection minimum resulted in the bergs' disappearance from satellite observations. Consequently, the temporal coverage of the drift of massive bergs is incomplete due to the largely unknown drift after break up, and the spatial coverage is limited to the western boundary current regions where these bergs are found.

A larger spatial coverage of drift tracks can be obtained by conventional technology, that is, tagging small to medium-size icebergs ($\leq$ 5 km edge length) which calve continuously. Size distributions observed by Budd *et al.* [1980] and Orheim [1980] determined edge maxima at 500 m and 1000 m with strong latitudinal dependence. Few icebergs of this size class were tagged in the 1970's [Tchernia and Jeannin, 1984; Vinje, 1980]. The drift of 21 icebergs, the majority tagged in the Indian and Pacific Ocean sectors of the Southern Ocean, reflected the path of the coastal current with retroflections corresponding to the main centres of atmospheric lows [Tchernia and Jeannin, 1984]. Vinje [1980] complemented these data with eight iceberg drift observations in the Weddell Sea. His study showed icebergs and sea ice reacting similarly to effects of wind in areas covered with sea ice and a steering influence of the sea-ice movement on the iceberg was suggested.

Various numerical studies of iceberg drift have addressed the impact of time- and space-variable ocean drag, wind drag, and Coriolis and other forces on the drift, for example Sodhi and El-Tahan [1980]; Gladstone *et al.* [2001]; Lichey and Hellmer [2001]. However, the latter demonstrated the dominant role of sea-ice concentration on iceberg drift: Whilst

ocean/wind drag and Coriolis force were found to be the most important driving forces in open water, modelled iceberg trajectories were closer to the observed drift of giant iceberg C7 when sea-ice concentration above 90% controlled the iceberg motion.

The objective of this study is to analyse the prevelant iceberg tracks in the Weddell Sea, to relate iceberg to sea-ice drift and to estimate the freshwater flux. For this purpose the Alfred Wegener Institute deployed 52 buoys on icebergs from January 1999 to January 2003 in the southwestern and southeastern Weddell Sea with the majority of bergs tagged off Neumayer station (70.6°S, 8.25°W, Fig.1). The buoys report daily GPS positions via the ARGOS system and a few buoys also transmit sea level pressure or air temperature data. This five year data set provides a detailed view of prevailing drift tracks and their variability in the Weddell Sea. Iceberg displacements were calculated from the position data and three zones determined to illustrate iceberg movements. The results were compared to previous basin-scale sea-ice drift studies by e.g. Wadhams *et al.* [1989]; Massom [1992]. The sea-ice/iceberg interaction was analysed using buoy arrays in the eastern and in the southwestern Weddell Sea. Direct information about iceberg behaviour during the austral winter in the northward-advancing sea-ice pack was obtained from an iceberg/sea-ice buoy array. Periods of coherent sea-ice/iceberg drift were identified as minima in the buoy kinematic time series. The freshwater flux was estimated from a combination of berg volumes (see iceberg dimensions in Table 1), observed drift patterns and modelled melt rates.

2. Data sampling and analysis

2.1. Iceberg buoys

Icebergs chosen for tagging were generally of length and width between 100 m and 1500 m, with freeboard heights between 10 m and 70 m, and drafts between 80 m and 550 m. Several larger icebergs were tagged, A43b being the largest, measuring 40000 m x 17000 m x 50 m (length x width x freeboard), which resulted from the calving events at the Filchner-Ronne Ice Shelf in 1998 (iceberg details are shown in Table 1). The origin of icebergs tagged in the southwestern Weddell Sea is well-known. The calving sites of icebergs marked in the eastern Weddell Sea and their prior drift is unknown.

52 icebergs were tagged opportunistically during five R/V Polarstern cruises which are referenced by date of deployment (e.g. Jan/99 for buoys released in January 1999). As R/V Polarstern supplies Neumayer Station once a year between November and March, the majority of buoys were placed on icebergs in the vicinity of Atka Bay (Fig. 1, inset). This enables seasonal as well as interannual differences in drift patterns to be determined. To cover a larger area an inhomogeneous distribution of buoys was sought when possible. This led to considerable variability in oceanographic and atmospheric conditions experienced by the icebergs monitored.

A deployment was considered after inspection of the iceberg surface. With crevasses present, large connected areas were sought to ensure a transmission of the buoy/iceberg-remains in case of break-ups. Usually this area was not located at the centre of the iceberg. Helicopter altimeter records gave height, GPS readings at the iceberg edges the size estimates.

The iceberg buoys transmitted their daily position (12:00 h) using the ARGOS satellite system. GPS positions were given with an accuracy of ± 15 m. If the GPS instrument failed ARGOS transmitter positions with an accuracy of 200 m to 300 m, depending on satellite availability, were recorded. Transmission and/or functionality problems sometimes resulted in position reports at varying times. Where necessary, interpolation routines were applied for a time interval between positions of 24 hours. Mean daily drift velocities were derived from the displacement between successive positions where u and v are the eastward and northward velocity components, respectively. An error of $\pm$ 1.4 $\cdot$ 10^{-3}m s^{-1} results from the accuracy of the sensor.

Buoys failing to transmit for more than two weeks were regarded as malfunctioning. Some of the newer generation of instruments recorded air pressure and/or air temperature with a sampling interval of 3 hrs, thus enhancing the sampling interval for iceberg position. Sea-level pressure and/or air temperature records were entered into the GTS system and used in the analysis model of the European Centre for Medium-range Weather Forcast (ECMWF). ECMWF wind velocity data were used to interpret the drift trajectories.

The data using daily position values do not resolve high frequency signals like the M_2-tide, the main component of tidal energy in the Weddell Sea [Robertson *et al.*, 1998]. However, they represent the overall drift pattern, as well as meso- and large-scale variability.

2.2. Sea-ice concentration

From March to September a roughly 1-m thick sea-ice cover is formed in the Weddell Sea which can extend to about 60°S, and to the west of the South Sandwich Islands farther north. During maximal sea-ice extent an area of $\sim$ 7.5 10^6 km^2 is covered. In

October/November the ice edge begins to retreat near Maud Rise (3°E,65°S). The area at minimal sea-ice cover in February/March is $\sim$ 1.5 10^6 km^2 with perennial sea-ice in the western Weddell Sea. The seasonal cycle of sea-ice cover lags the cycle of air temperature by two months. The interannual variability in sea-ice extent in the 80s and 90s was seen as a second mode wave pattern of the Antarctic Circumpolar Wave (ACW) with maxima every 4 years [White and Peterson, 1996].

Sea-ice concentrations before June 2003 were derived from SSM/I data using the 85 GHz channel using the ARTIST sea-ice (ASI) algorithm [Kaleschke *et al.*, 2001]. This provides a resolution of $\sim$ 15 km. From mid-2003 higher resolution data on a $\sim$ 5 km grid were available from AMSR-E (Advanced Microwave Scanning Radiometer for EOS). AMSR sea-ice concentrations were also calculated with ASI, using the 89 GHz channel. The ASI AMSR sea-ice concentration is slightly overestimated compared to the BOOTSTRAP algorithm, whereas the sea-ice edge is much better represented (*Spreen, pers. comm., 2004*). The pixel containing the iceberg buoy was taken to give the sea-ice concentration.

2.3. Differential kinematic parameters

To study the behaviour of iceberg movement with and within the sea-ice cover we calculated the time dependent, two dimensional horizontal flow field of several buoy arrays. Four triangular buoy arrays were available from the 52 buoys deployed for analysis. Two arrays (Sections 3.2 and 3.3) were assumed to represent the regional differences of iceberg movement within sea ice in the eastern and western Weddell Sea, and are presented here.

The deformation of the arrays were examined following Massom [1992] by using the change-of-area method. This provides four components of movement, i.e., divergence, vorticity, shear and stretch deformation referred to as differential kinematic parameter

(DKP). The method was developed by Saucier [1955] and used in the Southern Ocean for sea-ice kinematics by e.g. Wadhams *et al.* [1989]. The DKP components were compared with sea-ice concentrations and available atmospheric obervational and/or model data. The differential motion of a sea-ice field is related to changes in ice concentration. This in turn is related to atmospheric forcing events. Hence, icebergs "trapped" in large scale sea-ice fields should be seen as minima in DKP components. We assume that divergent and convergent movement is small when icebergs are in an area of high sea-ice concentration but large in open water conditions. The horizontal divergence D is expressed as the rate of change over time of a triangular area A which encloses the iceberg buoys:

$$D = \left(\frac{\partial u}{\partial x}\right) + \left(\frac{\partial v}{\partial y}\right) \simeq A^{-1}\frac{dA}{dt} = \frac{1}{A_0}\left[\frac{A_1 - A_0}{t_1 - t_0}\right] \tag{1}$$

with the areas A_0 and A_1 at times t_0 and t_1, respectively.

The vorticity, shear and stretch deformations can be calculated similarly using the rotation of the U and V vectors [Molinari and Kirwan, 1975; Wadhams *et al.*, 1989]. The physical interpretation of these parameters has been provided by Kirwan [1975]; divergence is the rate of area change without change in orientation or shape; vorticity is the rate of area change without change in shape or size; shear deformation is the rate of area change in shape due to forces acting parallel to the array sides (an elongated SE to NW axis is associated with negative, a shortened SW to NE axis with positive values), and stretch or normal deformation is the rate of elongation of the array, that is, compression or dilation along its NS and/or EW axis Massom [1992].

3. Iceberg drift

3.1. General features

An overview of drift patterns of the buoys deployed during five R/V Polarstern cruises is shown in Figure 2. The buoy trajectories follow the Weddell Gyre with a straight northward heading in the western part of the Weddell Sea and an eastward deflection at the northern tip of the Antarctic Peninsula. The drift in the eastern Weddell Sea is more intricate. Whilst the oceanic influence shows in meandering iceberg trajectories within the Coastal Current (CC), wind and possibly sea-ice influences can be seen as deviations from the northward progressing tracks [Sodhi and El-Tahan, 1980]. Buoy position records lasted for 3 to 1483 days. The calculated distances ranged from 7 km to 30.900 km. 19 % of the transmissions lasted for more than two years while 29 % ceased within half a year of deployment. The latter buoys were mainly deployed along the Greenwich Meridian (GM) north of 67°S. Observations made during deployment suggest that these icebergs were already eroded due to a prolonged drift and melt history leading to a shorter transmission period.

Buoy deployments during the Polarstern cruise in Jan/99 (Fig. 2(a)) were divided into three areas: The first along the GM on the way to Neumayer Station, the second off Neumayer Station, and the third in the southwestern Weddell Sea just off the Ronne Ice Shelf. As mentioned above, the iceberg buoys along the GM ceased transmitting soon after deployment (max. 70 days). Icebergs tagged off Neumayer followed the CC closely, two turned north in mid-April 1999 whereas one grounded and another moved farther south before turning northwards and then eastwards once north of 65°S. Icebergs tagged on the western continental shelf moved northward with mean speeds between 2.9 ± 4.3

km/day (westernmost track) and 9.5 ± 7.3 km/day (easternmost track). Whilst most of the icebergs took an easterly path when approaching the northwestern Weddell Sea following the Weddell Gyre, one buoy escaped into the Scotia Sea between Elephant and the South Orkney Islands. Although this is unique for Jan/99 buoys, all icebergs tagged in Jan/02 on the western continental shelf took this path, drifting into the Scotia Sea and beyond (Fig. 2(d)). This behaviour needs further investigation as it is still unclear what causes the icebergs to stay within the Weddell Sea, to follow the ACC fronts in the Scotia Sea or to head due north across the ACC fronts (see e.g. [Grosfeld *et al.*, 1998]).

Iceberg buoys in Jan/00, Dec/00 and Dec/02 were mainly deployed off Neumayer Station and in the CC to the east (Figs. 2(b,c,e)). The northward progression out of the CC usually occurred between March and May with a few exceptions where icebergs drifted due west into the Filchner Trough or across the southern Weddell Sea to the tip of the Antarctic Peninsula.

Whilst buoys deployed in Jan/00 dispersed broadly across the CC and subsequently covered a broad northward track out of it, a different behaviour was observed for buoys deployed in Dec/00 and Dec/02 with a more convergent buoy ensemble moving north at a similar longitude. The position and timing of discharge, as well as the northward direction taken, were determined by time and position of deployment, a result which agrees with the numerical study of Lichey and Hellmer [2001]. Bergs marked around 20°E reached the "critical" region later in the season thus experiencing a different wind field. These bergs tended to travel farther into the south-western Weddell Sea, similar to the temporarily grounded and larger icebergs. The dynamics of this behaviour still require further investigation.

The large-scale behaviour of the iceberg drift determines the interannual variability in iceberg export. Icebergs tagged in the eastern Weddell Sea needed approximately one seasonal cycle to reach the northern fringe of the Weddell Sea ($\sim 60°$S) and thus to export their freshwater to the north. At least two icebergs from those deployed in Jan/00 tended to complete a closed cycle in the Weddell Sea - one returned south with the Weddell Gyre east of 10°E but did not turn towards the west. For the other, the buoy ceased to transmit on its course south but spent the last ~ 90 days in ice-free conditions and seemed to follow a cyclonic circulation with a diameter of ~ 400 km. However, the onset of freezing and advance of the sea-ice edge would have worked against the southerly course. A different drift behaviour was prevalent in iceberg buoys released in Dec/00 and Dec/02 as they needed more than one seasonal cycle to reach 60°S. In fact, the Dec/00 icebergs took a sharp, almost 90°, turn east at the end of winter before being caught in the sea-ice of the next freezing season and subsequently transported north.

The overall drift pattern of individual buoys can be interpreted using their meander coefficient, which is the ratio of total distance covered to the overall displacement and thus a measure of directness of drift from point A to point B [Limbert *et al.*, 1989; Massom, 1992]. A minimum coefficient of one represent a straight path. In view of the circulation of the Weddell Gyre we divided the drift path into three sections, the Coastal Current (CC) with westward transport, the inner Weddell Sea (IW) with mainly northward transport, and the northern part of the Weddell Gyre and/or Scotia Sea (NW) with mainly eastward transport. The meander coefficients are presented in Table 2.

Low coefficients of 1.2 to 1.9 were found in the fast flowing CC which is directed west-southwest parallel to the coast and represents the southern branch of the Weddell Gyre.

The lack of any interannual variability may be caused by the similar deployment time in austral summer. Hence, with little sea-ice cover the bergs continued to drift with the CC until being forced northward presumably by atmospheric events. The only CC meander coefficient greater than 2, for buoy 9835 (Jan/00), may be the result of two cyclonic features in which the iceberg was trapped, resulting in an unusually low mean v-velocity of around 1 cm/s compared to 4 cm/s and above for other icebergs.

The western boundary current of the Weddell Gyre (part of the IW section) was also associated with low meander coefficients. From close to the Antarctic Peninsula up to roughly 45°W the values ranged from 1.6 to 2.4. Persistent southerly and southwesterly winds dominate the northward sea-ice drift and, in turn, that of icebergs enclosed in the sea-ice cover. The motion is interrupted by southward deviations during the passage of low pressure systems. Low values could indicate less atmospheric influence on the perennial sea-ice cover or, in the westernmost tens of kilometres, the closer proximity to more compact land-fast ice with higher viscosity.

Higher values along 40°W are in accordance with sea-ice buoy coefficients found in 1980 [Massom, 1992]. However, the largest coefficients were found in the eastern Weddell Sea for icebergs drifting north to the east of 35°W. Here, the sea-ice cover is unconsolidated owing to the frequent passage of atmospheric low-pressure systems across the area. Additionally, icebergs surviving more than one winter experience similar conditions again in the northern Weddell Sea, although the sea-ice conditions are variable and the effect less marked.

3.2. Western Weddell Sea (January - September 2002)

In this section, the main focus will be on iceberg # 9367 (length = 50 m, width = 250 m, freeboard = 25 m) visited in austral summer in the southern Weddell Sea while at the sea-ice edge (Fig. 3). In close proximity to this tagged iceberg three sea-ice buoys (see Kottmeier *et al.* [1997] for buoy specifications) were positioned (distance from # 9367 to # 8060: 62 km, to # 9728: 110 km, to # 9781: 145 km). A triangle of sea-ice and iceberg buoys reveals valuable information about the behaviour of the iceberg within the sea-ice. The northward advance of the sea-ice edge was faster than the northward progression of the sea-ice/iceberg buoy array. As sea-ice buoys deployed in 1980 showed a similar behaviour with respect to the ice edge advance we consider the thermodynamic process described by Massom [1992] to be the responsible force. The array's position remained at the sea-ice edge for only a few weeks before it was entrained in the pack ice.

All buoys were released just north of the continental shelf break and closely followed the continental slope on the way north (Fig. 3). The northward progression of the iceberg through/with the sea-ice can be separated into three sections. The southern part of the track from January to the end of March (Julian day 90) was characterised by a velocity of 6 $\pm$ 4 km/day with a sea-ice concentration of 68 $\pm$ 16 %. From April to mid-June the mean drift velocity within a mean coverage of 97 $\pm$ 3 % was 12.2 $\pm$ 7.5 km/day, and from mid-June to the end of the record, with a stronger eastward velocity component, mean progress was 17.5 $\pm$ 10.7 km/day. It is notable that the overall eastward transfer began (at day 175) when the tracks reached Joinville Ridge just south of Powell Basin. This latter behaviour, seen in iceberg as well as sea-ice buoy motion, seems to be a feature of the large scale oceanic circulation. From mid-March to mid-July iceberg and sea-ice

motion were in very good agreement. The drift velocities south of 70°S compare well with the iceberg motion determined by Vinje [1980] along 40°W.

Superimposed on the mean northward drift to 64°S, where a sharp eastward turn occurred, were two anticyclonic circulation features. The first began on 17 April and took 14 days for a complete cycle, the second started on 20 May and lasted for 4 to 7 days (Fig.3 right). Iceberg and sea-ice buoys turned south (2nd circle, west-south-west) retracing their path before heading north at almost the same location as 8 days (3 days) earlier. The main difference in drift tracks is the amplitude of the meridional (zonal) excursion. While the eastern buoys covered a N/S extent of 48 km, this was reduced to 36 km and 16 km for the western buoy, i.e., the amplitude of the excursion induced by the low pressure system decreased with increasing proximity to the shore. The E/W diameter of about 11 km varied by just 1 km between both pairs. Air temperatures recorded at buoy # 9781 at around day 120 - the time of the first anticyclonic feature - show a temperature rise to just below freezing point followed by a pressure decrease to 975 hPa and cold southerly winds. Northerly winds from the ECMWF model can be associated with warm temperatures, forcing the now consolidated (100 %) sea-ice cover and the iceberg southwards (Figure 4) and subsequent cold southerly winds with the northward continuation of the ensemble.

The second anticyclonic movement at around day 140 was ellipsoid in shape with the major E/W axis decreasing from 21 km at to 14 km (10 km) and thus becoming more circular in shape towards the west as the N/S axis changed only slightly in extent from 14 km to 9 km in the west. This westward change of amplitude and/or shape of circulation may be due to the transition to ice regimes with more compact conditions and thus higher viscosities. Sea-ice motion deduced from sea-ice buoy positions reveals a similar mean

progression for the period April to mid-June, decreasing slightly towards the west (# 8060 11.6 ± 7.6 km/day; #9781 10.6 ± 7.3 km/day and # 9728 9.8 ± 7.6 km/day). The coherence of the sea-ice buoy # 8060 and the iceberg drift patterns, despite a variation in the distance to the iceberg of about 34 ± 6 km during this period, is remarkable. The correlation between u and v velocity components of iceberg and sea-ice buoys for April, May, and June was striking with proportion of variance explained (r^2) above 0.94 (n$\simeq$90). For the v component of the entire track r^2 ranged from 0.84 to 0.89 while for the u component r^2 was 0.92 (n$\simeq$212).

As the buoy ensemble drifted northward the minimum air temperature increased (compared to lowest temperatures in May and June). However, temperatures were well below the ocean surface freezing point suppressing sea-ice melting for the entire drift. Towards the northern part of the drift warm temperature intrusions occurred about every 4 days, related to the passage of atmospheric low-pressure systems with the mean trough centred at around 64 °S [King and Turner, 1997].

The analysis of sea-ice concentration at the locations of the iceberg and the sea-ice buoys indicated that for 100 % sea-ice concentration a mechanical link existed between the drifters despite their being $\sim$ 30 km and more apart. Ice concentrations at the buoys ranged between 50 % and 80 % at the beginning of the drift and increased from day 87 to more than 90 % until the ensemble reached the northern Weddell Sea off Joinville Island where it entered the west wind zone. In fact, from April to mid-June sea-ice concentration at all four buoys was above 97 %. Thus, a high sea-ice concentration seems necessary for a coherent iceberg/sea-ice motion (Fig. 5) as proposed by Lichey and Hellmer [2001]. Low and fluctuating sea-ice concentrations at the beginning of the record reflect summer ice

conditions at the ice edge while the small fluctuations in sea-ice between April and June indicate the passage of synoptic low-pressure systems.

Figure 5b-e shows the DKP of the three-buoy ensemble # 9367, #8060, and #9781. The largest changes occurred between days 40 and 60 and can be associated with the shift of buoy position within the array. After the positions in the array were fixed by more compact sea-ice cover the divergence was small ($0.15\ 10^{-6} \pm 0.67\ 10^{-6}\ s^{-1}$) for the next 70 days. A change in shape occurred at the end of the anti-cyclonic motion at around day 120 due to negative shear, that is an elongated SE to NW axis (Fig. 5d), which is not represented as divergent motion of the array or in the vorticity. Since a cyclonic feature was observed at similar latitude and time of year during Ice Station Weddell (ISW) in 1992 [Geiger *et al.*, 1998], one might assume that both cyclonic movements are associated with features of bottom topography. However, they are related to atmospheric forcing acting on the sea-ice cover. ISW experienced wind shifts from northeast to southeast from day 116 to 121 while the Jan/02 iceberg/sea-ice buoy array experienced changes from southerly to northerly winds from day 112 to 121 with corresponding sea-ice and iceberg responses. The drift measured during ISW (5.8 km/day [Muench and Gordon, 1995]) situated approximately 6° farther west was slower than that of the Jan/02 buoy array (10.2 km/day for approximately the same latitude range) but agrees with the slower movement of the western buoy # 9728.

Although the second anticyclonic movement did not disturb the ensemble's progress, the entire ensemble turned sharply towards the west (10 days later at around day 153) and experienced vorticity and shear deformation (Fig 5c,d). This can be associated with a low pressure system (960 hPa, Fig 4a), with strong winds passing the buoy array. After

the ensemble turned east south of Powell Basin, sea-ice cover began to decrease (below 90 %) at around day 175 and a cyclonic circulation followed at around day 183. This cyclonic feature is associated with strong shear in DKP causing a new arrangement of the array with the SE-NW axis elongated and the SW-NE axis shortened (Fig 5d).

3.3. Eastern Weddell Sea (December 2000 - February 2002)

The data set of 11 icebergs tagged with buoys in Dec/00 was divided into two groups off Neumayer a) close to shore south of 69°S and b) farther off-shore (Fig. 1 - triangles). This can also be seen as a division between icebergs either surrounded by sea-ice or in ice-free waters at the beginning of the drift with one exception in a). Buoys deployed off-shore transmitted data for 25 to 154 days and drifted between 180 and 1000 km. The southern buoys followed the gyre rotation westward just north of the CC. Long periods spent in ice-free conditions leave icebergs vulnerable to melting and erosion as shown in model studies by Schodlok *et al.* [2005]. The transmissions of those buoys which followed the CC closely continued for up to two winters, transmitting positions for 432 to 807 days. The highest speeds in the core of the CC in the longitude range 9°W to 20°W were 31 km/day and 34 km/day decreasing to the north and south at $\sim$ 21 km/day and 10 km/day closest to the coast. Thus, in ice free conditions with the CC as leading driving force width of the CC of xxx km can be inferred by th

, reflecting slower currents close to the coast.

The three buoys # 25886, #25718, and # 25887 followed a coherent path from the end of March through October (Fig. 6) and, thus, were used to further investigate the iceberg drift behaviour in ice-covered seas. Although no sea-ice buoys were available, it was suggested in the previous section that SSM/I and AMSR-E data provide sea-ice

information which can be used for a similar analysis. The initial distance between buoys ranged from 40 to 90 km but diverged by up to 380 km in the first 100 days before decreasing to 42 to 120 km. This is reflected in a large variability in DKP values at the beginning of the drift followed by a calmer period interspersed with short-term events (Fig. 8b-e). The highly variable divergent/convergent patterns corresponded to low but highly variable sea-ice concentrations at the beginning of winter (Fig. 8a). In mid-March the sea-ice cover consolidated to more than 90 % in the vicinity of the icebergs. Temperatures below zero fuelling sea-ice growth and the northward advance of sea-ice from the southwestern Weddell Sea both contributed to the high concentration. Two turning points determined the drift track of the buoy ensemble, associated with the discharge of the icebergs from the CC (Fig 6) into the inner Weddell Sea and the departure from the mean northward course towards the east (note the 90° turn east at day 577).

Drift velocities in the CC before turning north were lower for # 25887 (8.6 ± 4.3 km/day) than for the other two icebergs (12.4 ± 5.9 km/day and 11.6 ± 6.9 km/day) although mean u and v velocity components were similar. The southwestward drift within the CC followed the irregular topography causing some meandering but without deviations related to atmospheric events, e.g., catabatic winds from the continental plateau. Atmospherically forced deviations and/or reversals occurred regularly during the northward progression and started in the turning area off the Eastern Weddell Ice Shelves (20°W - 24°W and 72°S - 73°S). Thus, the north turn occurred within 14 days (day 427 to day 440) before a stable ensemble array was established. The question whether the northward turn was due to atmospheric events, ice conditions and/or iceberg size is beyond the scope of this paper but will be pursued in another study.

The general northwestward progression of the ensemble showed several significant departures from the mean drift, anticyclonic loops south of 70.5°S followed by cyclonic loops to the north. The overall drift behaviour of all buoys was rather coherent with mean speeds of 11.3 ± 6.8 km/day (# 25887) to 11.6 ± 7.0 km/day (# 25886). The largest departure of the ensemble from the mean track was a 20 day N-NE excursion of ∼ 145 km caused by a change from southeasterly to southwesterly winds and an increase in strength. With a wind change to more northerly directions the course of the ensemble reversed, tracing back within 50 km north of the point of origin. The other features were more circular, ranging from 10 km/20 km to 40 km/60 km in NS/EW extent, and loop cycles lasted between 10 and 16 days.

Taking the correlation between u and/or v buoy velocities as a measure of coherence, the relationship between percentage sea-ice cover and coherent drift of icebergs and sea-ice was examined. There was no discernible relationship for the period from December to March with highly variable sea-ice concentration. However, the proportion of variance in coherence explained by sea-ice cover exceeded 0.8 (n > 200) when sea-ice concentration was above 86 % in the period from the end of March to October. The correlation between u and v velocity components of the icebergs for end of March through October was even stronger, with r^2 above 0.95 (n≃215) for the u and v components. The horizontal ECMWF wind and iceberg buoy velocities were likewise well correlated with r^2 above 0.85 (n=215), i.e., wind acting on the sea-ice cover indirectly forced the iceberg motion.

DKP values during the entire coherent track were again small (0.05 10^{-6} to 0.06 10^{-6} s^{-1}), suggesting a mechanical link to the sea ice. Deviations from the mean northward course were associated with perturbations in DKP, the largest of which occurred just

before the turn eastwards around day 574. Whereas convergent followed by divergent movement remained small, vorticity, shear and stretch deformation deviations were large at the beginning and end of track. A low pressure system with 975 hPa (Fig. 7) and warmer temperatures from the north could be associated with this event, and the high pressure system (1005 hPa) passing a few days later coincided with the eastward turn. However, mean atmospheric pressure along the track was rather low at 986 hPA $\pm$ 12 hPa, and rarely exceeded 1000 hPa. Other than the largest perturbation in DKP values at day 574 several smaller disturbances could be also associated with atmospheric events. The buoy ensemble experienced positive shear deformation, negative stretch deformation and vorticity at day 490 while the anti-cyclonic movement at day 551 was accompanied by little shear and large stretch deformation. The former date marked the day on which the 145 km N-NE excursion started and winds shifted from southeast to southwest, the latter was at the end of the following cyclonic circulation associated with southeasterly winds and the mean northwestward progression of the ensemble.

The drift speed in the predominantly eastward progression after day 577 along 67°S ranged from 10.2 $\pm$ 7.3 km/day to 13.1 $\pm$ 8.6 km/day with mean ice concentrations still above 85 %. However, at the end of winter with no recent ice formation such high sea-ice concentration close to the icebergs (Fig. 8a) was due to advection from the southeast. Leads within the ice pack had formed and reflect the open water portion of the satellite pixel but not necessarily the mechanical link to adjacent icebergs. While the first sea-ice season lasted for 295 to 315 days, the second was considerably shorter at 230 to 250 days (not shown here). At the end of the second winter the northeastward progression of the icebergs (Fig. 2c) worked against the southward retreat of the sea-ice due to melting,

reducing the residence time in sea-ice covered waters. The DKP variability was still small until day 660, at which time sea-ice concentration decreased to well below 85 % coinciding with the end of the coherent behaviour (see Fig. 6 end of red curve - buoy # 25887). While the distance between buoys # 25886 and # 25887 increased slowly from 100 to 200 km up to day 660, it subsequently increased to 300 km within a few days. This suggests that the length scale at which coherent motion occurs is smaller than 300 km. Buoys # 25886 and # 25827 showed a rather constant distance of $\sim$ 100 km which increased only slightly to $\sim$ 120 km.

The two northern buoys drifted onwards farther east whereas the southern buoy turned north before its eastwards progress causing large DKP values and a rearrangement of the array. The two southern icebergs of the three-berg ensemble survived the summer and, thus, the sea-ice-free period ($\sim$ 100 days) drifting nearly parallel northward once enclosed again in the sea-ice cover. With more variable sea-ice conditions during this northward drift and a position closer to the sea-ice edge, the drift pattern is not as coherent as during the first sea-ice season.

3.4. Freshwater Export

Iceberg volume in the Weddell Sea is a balance between the calving rate within the Weddell Sea, import from the east and export to the north. Taking a mean iceberg calving rate of 410 Gt/a in the Weddell Sea [Gladstone *et al.*, 2001] the tagged icebergs are equivalent to less than 3% of this flux. The calving of huge tabular icebergs is not taken into consideration. Iceberg A43b tagged in 2002 represents 88 % of this rate and thus a higher calving rate can be assumed in this year. Although one has to consider that only a minor portion of icebergs entering the Weddell Sea from the east were tagged with

buoys and that a significant number of bergs calving from Weddell Sea ice fronts move out of the region, we assume that the tagged bergs give a representative picture of export patterns from the Weddell Sea. These can be summarized in three scenarios:

(1) complete export of tagged icebergs (Fig. 2a,d),

(2) partial export to the north with some bergs remaining in the Weddell Gyre for more than one year (Fig. 2c), and

(3) all tagged icebergs remain in the Weddell Gyre (Fig. 2b).

In order to give a first estimate of the freshwater budget for each scenario, we assume that import from the east into the eastern Weddell Sea is compensated by export to the north, and write the equation:

C (Calved iceberg volume) = F (Volume melted in the WS) + E (Volume exported from the WS) + R (Solid ice remaining in the WS) [**1**]

where the melted volume F can be approximated as F = Cm the product of calved volume (C) and the proportion (m) of melted to initial volume of an average sized iceberg with a melt rate (r). The three scenarios correspond to the assumptions: (1) R = 0, (2) E,R $>$ 0 and (3) E = 0. For the simplest scenario (3), the 410 Gt/a in the Weddell Sea are equivalent to a freshwater flux of $\sim$ 15.3 mSv (ρ_{ib} = 850 kg m^{-3}). This corresponds to about 40% of the NCEP reanalysis P-E input into the Weddell Sea and is comparable to the ice shelf basal melting [Hellmer, 2004].

For an estimate of the proportion of an iceberg that melts during the transit of the Weddell Sea the iceberg size, thickness and drift time are provided from the tagged icebergs. The median of observed iceberg area is A_{mdn} = 0.26 km^2, the mean iceberg draft 330 m (Table 1), and the mean iceberg transit time t_{WS} = 1 year. The iceberg melting rate (r)

was taken from drift/melt model based on Lichey and Hellmer [2001]. The latter model was improved through implementing the wave radiation force as a supplemental driving force, and iceberg decay was parameterised through basal and lateral melt following **?** wave erosion following Gladstone *et al.* [2001]. The freshwater input showed an increase of meltwater from a minimum of 4 m a^{-1} at the iceshelf front to a maximum of 90 m a^{-1} in the Scotia Sea near the South Orkney Islands [Schodlok *et al.*, 2005; Morgan and Budd, 1978]. The mean value r in the central Weddell Sea is 25 m a^{-1} and was choosen to be representative for the inner Weddell Sea with most of tracks covered. This results in a proportion m = 0.0757. With 410 Gt/a as calved iceberg volume (C) the calculated freshwater input is F = 31 Gt/a. Substituting these values into Eqn. 1 the freshwater budgets for the different scenarios are:
(1) E = 368 Gt/a, (2) E = R = 184 Gt/a (assuming a 50:50 split between export and remainder), and (3) R = 368 Gt/a.

The export dominates melting in scenarios (1) and (2), and the large values for fraction R in scenarios (2) and (3) confirm that the Weddell Sea freshwater budget is profoundly influenced by the export scenarios in a given year. In addition, the drift tracks obtained from this study suggest that the freshwater released is not only confined to the Coastal Current as suggested by Gladstone *et al.* [2001] but spread across the Weddell Sea.

4. Discussion and Conclusions

The outstanding feature of the tagged icebergs is the coherent movement during parts of their drift. Vinje [1980] showed an example of three nearly parallel northward drifting icebergs between 10°W and 20°W within 6/8 to 8/8 sea-ice cover which corresponds to 75% to 100 % in SSM/I AMSR - deduced concentrations. However, a high uncertainty in the

sea-ice concentration has to be taken into account for these values due to lower resolution in the early satellite technology. The observations presented in this study provide the first evidence in support of model results of Lichey and Hellmer [2001], confirming that coherent sea-ice/iceberg motion occurs only at sea-ice concentrations above a certain threshold. In the two studies of iceberg and sea-ice buoy arrays and high resolution, satellite-derived sea-ice concentration which could be carried out using the data set to date, the threshold was found to be 86 % in the eastern Weddell Sea and 93 %, in the western Weddell Sea with the perennial sea-ice cover. These results are in broad agreement with the threshold of 90% found by Lichey and Hellmer [2001], and indicate that the threshold itself may be sensitive to the dominant physical processes in a given area. The conformity in northward/eastward motion is due to the steering influence of the highly consolidated sea-ice cover, which in turn is controlled by the atmospheric pressure systems prevailing in this area. Cyclonic activities occurred frequently along the tracks with even lower pressures in the eastern Weddell Sea. The long-term motion of sea-ice and icebergs agreed with the course of the Weddell Gyre. Only during northerly winds the general drift was temporarily reversed as also shown by Thomas *et al.* [1995]. Massom [1992] found a coherence of movement in sea-ice buoys separated by more than 100 km. In this study buoys separated by 50 - 150 km (western Weddell Sea) and 80 - 240 km (eastern Weddell Sea), responded in a coherent manner to the passage of atmospheric low-pressure systems. Thus, the buoy arrays suggest a length scale of less than 250 km in which coherent motion of the sea-ice cover occurs; in the Arctic Ocean this length scale is proposed to be 400 km [Thorndike, 1986].

ISW drift rates in the western Weddell Sea, iceberg observations in the central Weddell Sea [Vinje, 1980], and the buoy drifts presented here compare well with mean drifts of the ships *Deutschland* (6.0 km/day, 32°W - 45 °W) and *Endurance* (4.3 km/day, 50°W - 53°W) [Gordon *et al.*, 1981]. Fastest drifts occurred in the CC off Neumayer with mean speeds of $\sim$ 34 km/day and maxima of up to 50 km/day. Satellite observations of icebergs off Dronning Maud Land drifting in the CC showed a westward intensification in speed [Aoki, 2003]. Our data do not show this westward intensification west of 10°W. However, the speed of buoy # 25718 is well above that of iceberg B9A in the same area, without consideration of seasonality possibly reflecting the interannual variability of the Coastal Current.

Observations show a considerable interannual variation in drift speed and direction. The drift of icebergs in ice-free water mainly represents the forcing effects of the upper 200-400 m of the water column caused by the large keel, whereas in consolidated ice the influence of the wind on the sea-ice cover and, in turn, on the iceberg drift is more important. The iceberg, i.e., freshwater export out of the Weddell Sea is determined by the berg's discharge out of the CC and the survival period for one or two winter seasons but does not depend on routes within the Weddell Sea. At the tip of the Antarctic Peninsula two routes have been observed with little knowledge about the dynamics controlling the preferred tracks. Most of the icebergs drifting over the western Weddell Sea continental shelf are exported into the Scotia Sea between Elephant and South Orkney Islands while IPAB sea-ice buoys released from 1986 to 2000 followed the Weddell Gyre eastwards [Schmitt *et al.*, 2004]. Whether this suggests a decoupling of sea-ice and iceberg motion in low sea-ice concentrations at the tip of the Antarctic Peninsula or is due to the fact of limited

sea-ice buoy data needs to be further investigated in terms of dynamics, seasonality and/or interannual variability. Icebergs drifting in the central and/or eastern Weddell Sea either join the eastward flow of the ACC or stay in the northern branch of the Weddell Gyre with the potential to turn southwards in the gyre recirculation. The latter means that no freshwater is exported from the Weddell Sea. A complete cycle within the Weddell Gyre was not observed with the buoys in this study. Indeed, no such observations, e.g. from ARGOS Floats, have been reported to date. However, numerical studies suggest that recirculation of the Weddell Gyre with its double cell structure is a subsurface expression [Beckmann *et al.*, 1999].

Iceberg volume in the Weddell Sea is a balance between the calving rate within the Weddell Sea, import from the east and export to the north. Taking a mean iceberg calving rate of 410 Gt/a in the Weddell Sea [Gladstone *et al.*, 2001] the tagged icebergs are equivalent to less than 3% of this flux. The calving of huge tabular icebergs is not taken into consideration. Iceberg A43b tagged in 2002 represents 88 % of this rate and thus a higher calving rate can be assumed in this year. Although one has to consider that only a minor portion of icebergs entering the Weddell Sea from the east were tagged with buoys and that a significant number of bergs calving from Weddell Sea ice fronts move out of the region, we assume that the tagged bergs give a representative picture of export patterns from the Weddell Sea. These can be summarized in three scenarios:

(1) complete export of tagged icebergs (Fig. 2a,d),

(2) partial export to the north with some bergs remaining in the Weddell Gyre for more than one year (Fig. 2c), and

(3) all tagged icebergs remain in the Weddell Gyre (Fig. 2b).

In order to give a first estimate of the freshwater budget for each scenario, we assume that import from the east into the eastern Weddell Sea is compensated by export to the north, and write the equation:

C (Calved iceberg volume) = F (Volume melted in the WS) + E (Volume exported from the WS) + R (Solid ice remaining in the WS) **[1]**

where the melted volume F can be approximated as F = Cm the product of calved volume (C) and the proportion (m) of melted to initial volume of an average sized iceberg with a melt rate (r). The three scenarios correspond to the assumptions: (1) R = 0, (2) E,R > 0 and (3) E = 0. For the simplest scenario (3), the 410 Gt/a in the Weddell Sea are equivalent to a freshwater flux of $\sim$ 15.3 mSv (ρ_{ib} = 850 kg m^{-3}). This corresponds to about 40% of the NCEP reanalysis P-E input into the Weddell Sea and is comparable to the ice shelf basal melting [Hellmer, 2004].

For an estimate of the proportion of an iceberg that melts during the transit of the Weddell Sea the iceberg size, thickness and drift time are provided from the tagged icebergs. The median of observed iceberg area is A_{mdn} = 0.26 km^2, the mean iceberg draft 330 m (Table 1), and the mean iceberg transit time t_{WS} = 1 year. The iceberg melting rate (r) was taken from drift/melt model based on Lichey and Hellmer [2001]. The latter model was improved through implementing the wave radiation force as a supplemental driving force, and iceberg decay was parameterised through basal and lateral melt following **?** wave erosion following Gladstone *et al.* [2001]. The freshwater input showed an increase of meltwater from a minimum of 4 m a^{-1} at the iceshelf front to a maximum of 90 m a^{-1} in the Scotia Sea near the South Orkney Islands [Schodlok *et al.*, 2005; Morgan and Budd, 1978]. The mean value r in the central Weddell Sea is 25 m a^{-1} and was choosen

to be representative for the inner Weddell Sea with most of tracks covered. This results in a proportion m = 0.0757. With 410 Gt/a as calved iceberg volume (C) the calculated freshwater input is F = 31 Gt/a. Substituting these values into Eqn. 1 the freshwater budgets for the different scenarios are:
(1) E = 368 Gt/a, (2) E = R = 184 Gt/a (assuming a 50:50 split between export and remainder), and (3) R = 368 Gt/a.

The export dominates melting in scenarios (1) and (2), and the large values for fraction R in scenarios (2) and (3) confirm that the Weddell Sea freshwater budget is profoundly influenced by the export scenarios in a given year. In addition, the drift tracks obtained from this study suggest that the freshwater released is not only confined to the Coastal Current as suggested by Gladstone *et al.* [2001] but spread across the Weddell Sea.

For future studies, sea-ice / iceberg buoy arrays are needed with a higher temporal position transmission rate in order to demonstrate whether the 90 % coherence threshold and length scale assumptions are appropriate for the whole Weddell Sea. The effects of waves and tides need to be taken into account by adding more sensors, including strain and tilt, to the buoy for a better understanding of the iceberg decay. The latter is essential for determining a significant component of the Southern Ocean freshwater budget. Preferred drift tracks reported in this study combined with model results used as boundary conditions for melting can provide a more detailed estimate of the freshwater input to the water column of the Weddell Sea and/or export out of the region.

Acknowledgments. We are grateful to J. Schwarz and S. Marsland for helpful discussions to improve this manuscript, thankful to L. Kaleschke and G. Spreen for providing the SSM/I and AMSR-E sea-ice data (www.seaice.de), and also thank H. Rohr, L. Sell-

mann and M. Kruse for processing the ARGOS data. This study was partially founded by Deutsche Forschungsgemeinschaft (HE 2881/1-1)

References

Aoki, S. (2003). Seasonal and spatial variations of iceberg drift off Dronning Maud Land, Antarctica, detected by satellite scatterometers. *J. Oceanogr.*, *59*, 629–635.

Beckmann, A., Hellmer, H. H., and Timmermann, R. (1999). A numerical model of the Weddell Sea: large scale circulation and water mass distribution. *J. Geophys. Res.*, *104*, 23375–23391.

Budd, W. F., Jacka, T. H., and Morgan, V. I. (1980). Antarctic iceberg melt rates derived from size distributions and movement rates. *Annals of Glaciology*, *1*, 103–112.

Budd, R. E. (1935). Discovery: The story of the second Byrd Antarctic expedition. *G. P. Putnam's Sons*, *New York*, 405 pages.

GEBCO (2003). Centenary Edition of the GEBCO Digital Atlas. published on CD-ROM on behalf of the IOC and IHO as part of the General Batymetric Chart of the Oceans, BOCD, Liverpool.

Geiger, C., Ackley, S., and Hibler, W. (1998). Sea ice drift and deformation processes in the western Weddell Sea. In M.O. Jeffries, editor, *Antarctic Sea Ice: Physical processes, interaction and variability*, volume **74** of *Antarc. Res. Ser.*, pages 141–160. AGU.

Gladstone, R., Bigg, G. R., and Nicholls, K. W. (2001). Icebergs trajectory modelling and meltwater injection into the Southern Ocean. *J. Geophys. Res.*, *106*, 19903–19915.

Gladstone, R. and Bigg, G. R. (2002). Satellite tracking of icebergs in the Weddell Sea. *Antarc. Sci.*, *14*, 278–287.

Gordon, A., Martinson, D. G., and Taylor, H. (1981). The wind-driven circulation in the Weddell-Enderby-Basin. *Deep-Sea Res.*, *28*, 151–163.

Grosfeld, K., Hellmer, H., Jonas, M., Sandhäger, H., Schulte, M., and Vaughan, D. (1998). Marine ice beneath Filchner Ice Shelf: evidence from a Multi-disciplinary approach. In S.S. Jacobs and R.F. Weiss, editor, *Ocean, Ice, and Atmosphere: Interactions at the Antarctic Continental Margin*, volume **75** of *Antarc. Res. Ser.*, pages 319–339. AGU.

Grosfeld, K., Schröder, M., Fahrbach, E., Gerdes, R., and Mackensen, A. (2001). How iceberg calving and grounding change the circulation and hydrography in the Filchner Ice Shelf-Ocean System. *J. Geophys. Res.*, *106*, 9039–9055.

Gutt, J. and Starmans, A. (2001). Quantification of iceberg input and benthic recolonisation patterns in the Weddell Sea (Antarctica). *Polar Biol.*, *24*, 615–619.

Hellmer, H. H. (2004). Impact of Antarctic ice shelf melting on sea ice and deep ocean properties. *Geophys. Res. Let.*, *31*(10), L10307, DOI: 10.1029/2004GL19506.

Hellmer, H. H., S. S. Jacobs, and Jenkins, A. (1998). Oceanic erosin of a floating Antarctic glacier in the Amundsen Sea. In S.S. Jacobs and R.F. Weiss, editor, *Ocean, Ice and Atmosphere: Interactions at the Antarctic Continental Margin*, volume **75** of *Antarc. Res. Ser.*, pages 83–99. AGU.

Jacobs, S. S., Hellmer, H. H., Doake, C. S. M., Jenkins, A., and Frolich, R. M. (1992). Melting of ice shelves and the mass balance of Antarctica. *J. Glaciol.*, *38*, 375–387.

Kaleschke, L., Lüpkes, C., Vihma, T., Haarpainter, J., Borchert, A., Hartmann, J., and Heygster, G. (2001). SSM/I sea ice remote sensing for mesoscale Ocean-Atmosphere interaction analysis. *Can. J. Rem. Sens.*, *27*(5), 526–537.

King, J. C. and Turner, J. (1997). *Antarctic meteorology and climatology*. Cambridge University Press.

Kirwan, A. (1975). Ocean velocity gradient. *J. Phys. Oceanogr.*, *5*, 729–735.

Kottmeier, C., Ackley, S., Andreas, E., Crane, D., Hoeber, H., King, J., und D. Limbert, J. L., Martinson, D., Roth, R., Sellmann, L., Wadhams, P., and Vihma, T. (1997). Wind, temperature and ice motion statistics in the Weddell Sea. *WMO/TD*, *979*, 48.

Lichey, C. and Hellmer, H. H. (2001). Modeling giant iceberg drift under the influence of sea ice in the Weddell Sea. *J. Glaciol.*, *47*, 452–460.

Limbert, D., Morrison, S., Sear, C., Wadhams, P., and Rowe, M. (1989). Pack-ice motion in the Weddell Sea in relation to weather systems and determination of a Weddell Sea sea ice budget. *Annals of Glaciology*, *12*, 104–112.

Massom, R. (1992). Observing the advection of sea ice in the Weddell Sea using buoy and satellite passive microwave data. *J. Geophys. Res.*, *97*(10), 15559–15572.

Molinari, R. and Kirwan, A. (1975). Calculations of differential kinematic properties from Lagrangian observations in the western Caribbean Sea. *J. Phys. Oceanogr.*, *5*, 483–491.

Morgan, V. I. and Budd, W. F. (1978). The distribution and melt rates of Antarctic icebergs. In Husseiny, A. A. (ed), *Iceberg utilization*, *Proceedings of the first International Conference, Ames, Iowa, 1977*, pages 220–228. Pergamon Press, New York.

Muench, R. D. and Gordon, A. L. (1995). Circulation and transport of water along the western Weddell Sea margin. *J. Geophys. Res.*, *100*, 18503–18515.

Nøst, O. A. and Østerhus, S. (1998). Impact of grounded icebergs on the hydrographic conditions near the Filchner Ice Shelf, Antarctica. In S.S. Jacobs and R.F. Weiss, editor, *Ocean, Ice and Atmosphere: Interactions at the Antarctic Continental Margin*,

volume **75** of *Antarc. Res. Ser.*, pages 269–286. AGU.

Orheim, O. (1980). Physical characteristics and life expectancy of tabular antarctic icebergs. *Annals of Glaciology*, *1*, 11–18.

Robertson, R. L., Padman, L., and Egbert, G. D. (1998). Tides in the Weddell Sea. In S.S. Jacobs and R.F. Weiss, editor, *Ocean, Ice and Atmosphere: Interactions at the Antarctic Continental Margin*, volume **75** of *Antarc. Res. Ser.*, pages 341–369. AGU.

Saucier, W. (1955). *Principles of meteorological analysis*. University of Chicago Press.

Schmitt, C., Kottmeier, Ch., Wassermann, S., and Drinkwater, M., 2004 *Atlas of Antarctic Sea Ice Drift*. http://imkhp7.physik.uni-karlsruhe.de/∼eisatlas/HTML/eisatlas_buoys.html

Schodlok, M. P., Hellmer, H. H., Schwarz, J. N., and Busche, T. (2005). On iceberg behaviour: observations, model results and satellite data. *FRISP Report No.* **16**. Bjerknes Centre for Climate Research, Bergen, Norway. in press.

Sodhi, D. S. and El-Tahan, M. (1980). Prediction of an iceberg drift trajectory during a storm. *Annals of Glaciology*, *1*, 77–82.

Swithinbank, C., McClain, P. and Little, P. (1984). Drift tracks of Antarctic icebergs. *Polar Rec.*, *18*, 495–501.

Tchernia, P. and Jeannin, P. F. (1984). Circulation in Antarctic waters as revealed by iceberg tracks 1972–1983. *Polar Rec.*, *22*, 263–269.

Thomas, J. P., Turner, J., Lachlan-Cope, T. A., and Corcoran, G. (1995). High resolution observations of Weddell Sea surface currents using ERS-1 SAR sea-ice motion vectors. *Int. J. Remote Sensing*, *16*, 3409–3425.

Thorndike, A. S. (1986). Kinematics of sea ice. In N. Untersteiner, editor, *The geophysics of sea ice*, volume **146** of *NATO ASI Series B: Physics*, pages 489–550. Plenum Press, New York.

Vihma, T., Launiainen, J., and Uotila, J. (1996). Weddell Sea ice drift: Kinematics and wind forcing. *J. Geophys. Res.*, *101*, 18279–18296.

Vinje, T. E. (1980). Some satellite-tracked iceberg drifts in the Antarctic. *Annals of Glaciology*, *1*, 83–87.

Wadhams, P., Sear, C., Crane, D., Rowe, M., Morrison, S., and Limbert, D. (1989). Basin-scale ice motion and deformation in the Weddell Sea during winter. *Annals of Glaciology*, *12*, 178–186.

Weeks, W. F. and Campbell, W. J. (1973). CRREL Research Report 200. *U.S. Army Cold Reg. Res. Eng Lab., Hanover, New Hampshire.*

Weeks, W. F. and Mellor, M. (1978). *Proc. Int. Conf. Iceberg Util., 1st*, 45–98.

White, W. B. and Peterson, R. G. (1996). An Antarctic circumpolar wave in surface pressure, wind, temperature and sea–ice extent . *Nature*, *380*, 699–702.

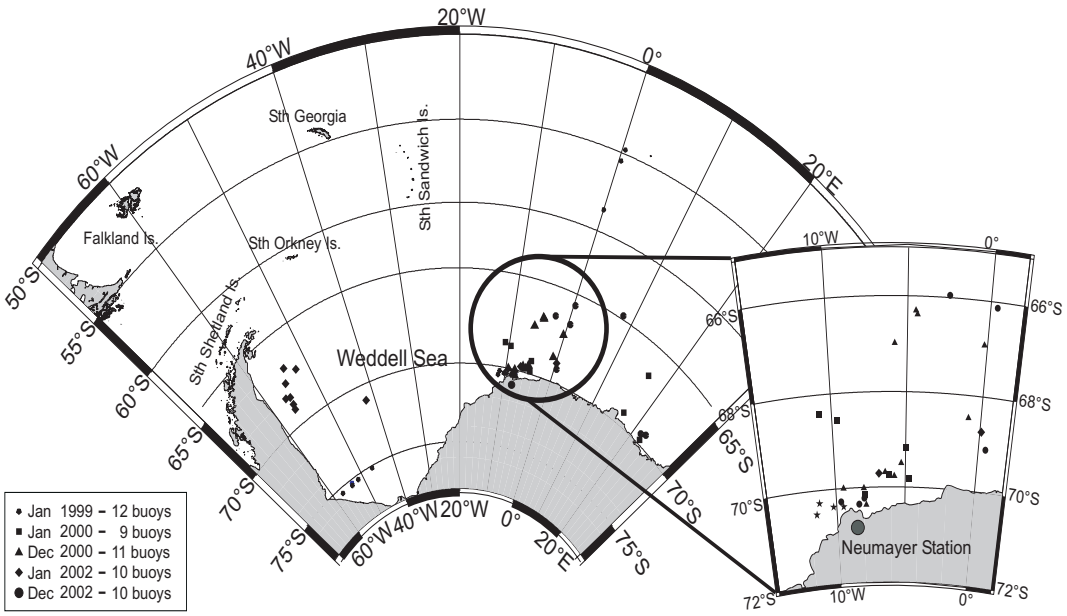

Figure 1. Dates, positions, and number of buoys deployed in the Weddell Sea during five cruises of R/V Polarstern. The majority of buoys were released off Neumayer Station (inset).

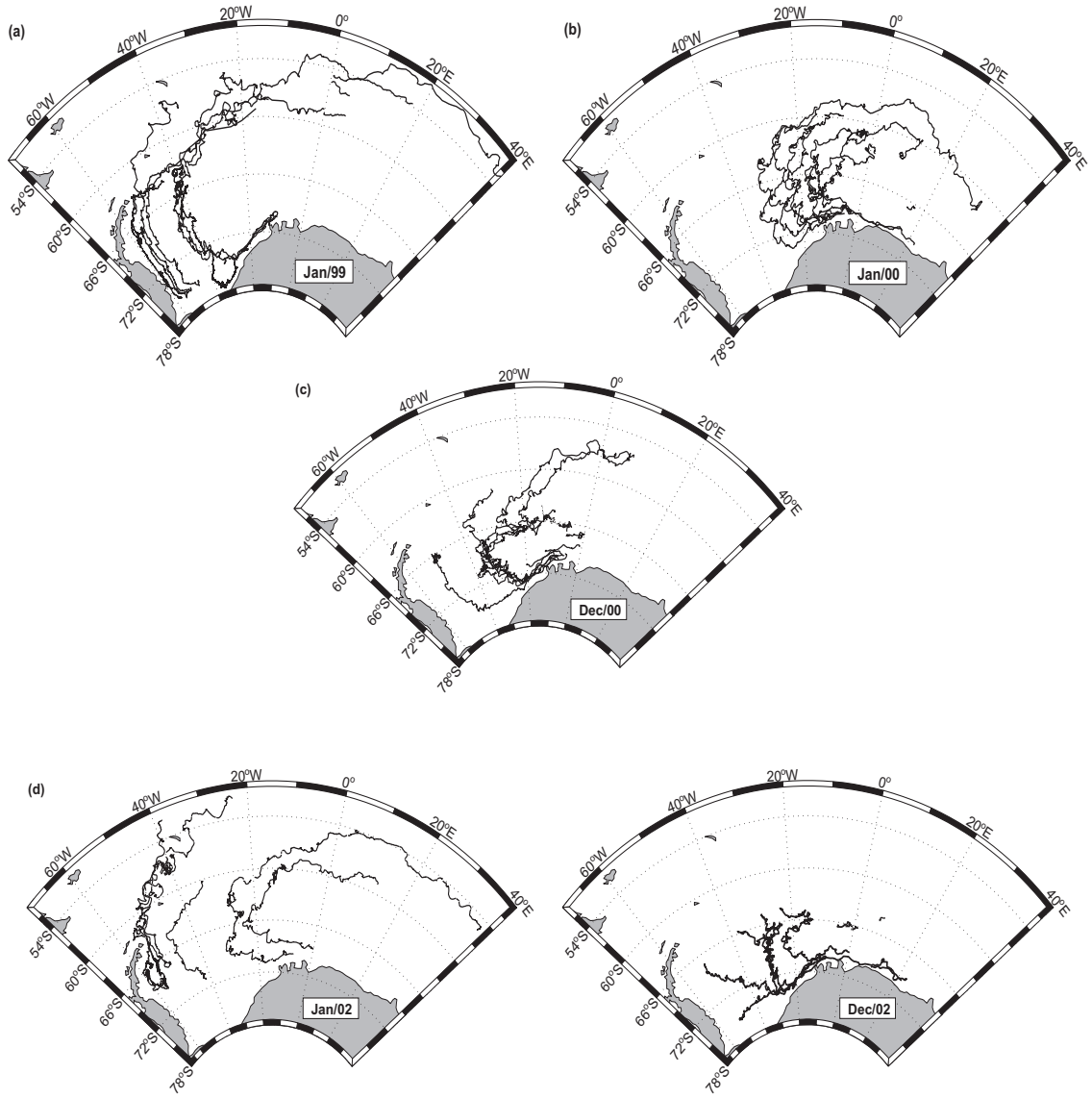

Figure 2. Drift tracks of icebergs in the Weddell Sea tagged with buoys deployed in January 1999 (a), January 2000 (b), December 2000 (c), January 2002 (d) and in December 2002 (e). The labels, e.g. Jan/99, refer to Month and Year of deployment.

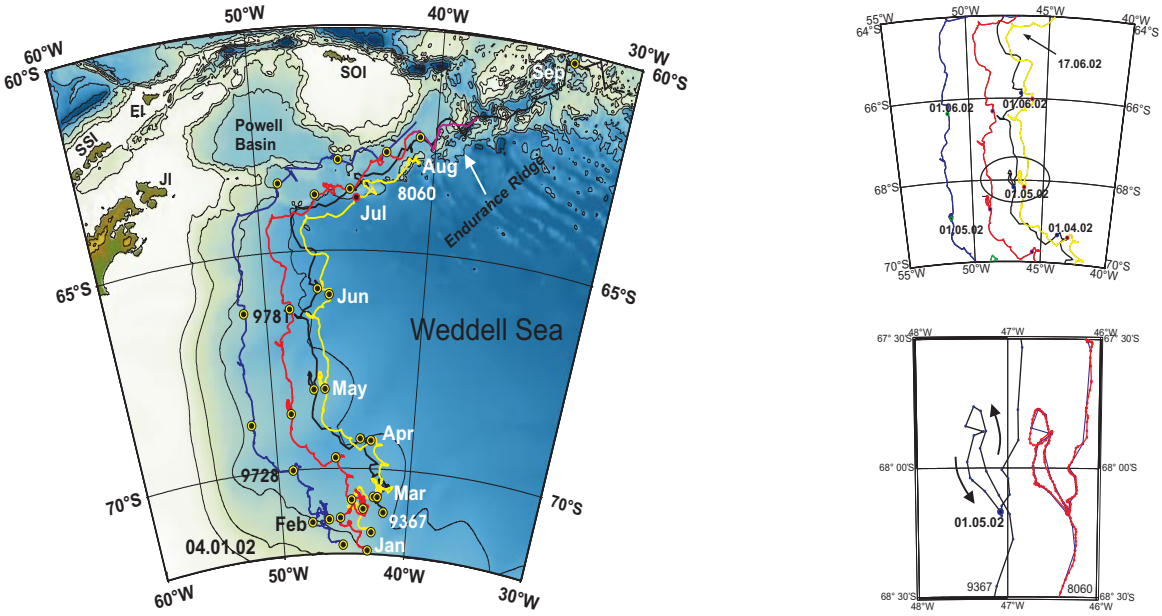

Figure 3. Left: Drift patterns of iceberg # 9367 (black) and sea-ice buoys # 8060 (yellow), # 9781 (red), and # 9728 (blue) from point of deployment in January 2002 to August 2002. Iceberg data are available until the beginning of September, and sea-ice buoy until the end of July. The bottom topography is derived from the GEBCO 1-min [GEBCO, 2003] data set with isopleths shown at 1000 m intervals. Abbreviations: EI - Elephant Island, JI - Joinville Island, SOI - South Orkney Islands, and SSI - South Shetland Islands. Right: Iceberg and sea-ice buoy drift patterns from April to July 2002 (top). Comparison between iceberg path (#9367) with 24-h sampling interval and sea-ice buoy # 8060 with 3-h sampling interval for the circled area in top panel (bottom). The blue tracks represent the daily buoy positions at noon, 3 hourly sea-ice buoy positions are overlain in red.

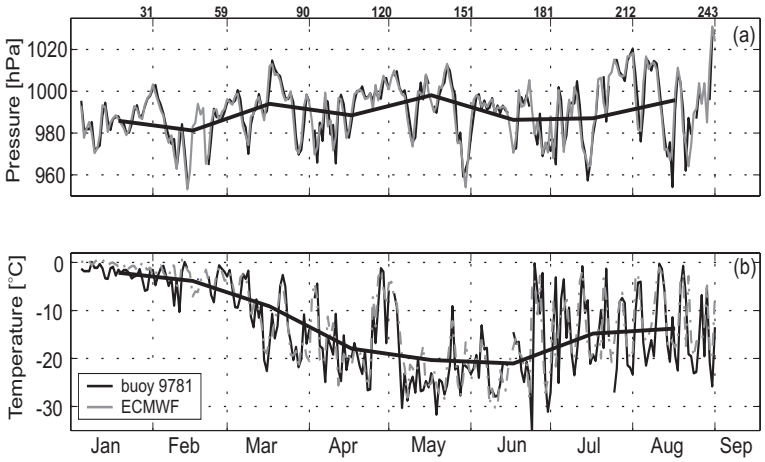

Figure 4. a) Pressure vs time and b) temperature vs time recorded at buoy # 9781 close to iceberg # 9367 representing atmospheric conditions during the drift through the western Weddell Sea. The solid curve in a) and b) represents the monthly mean value.

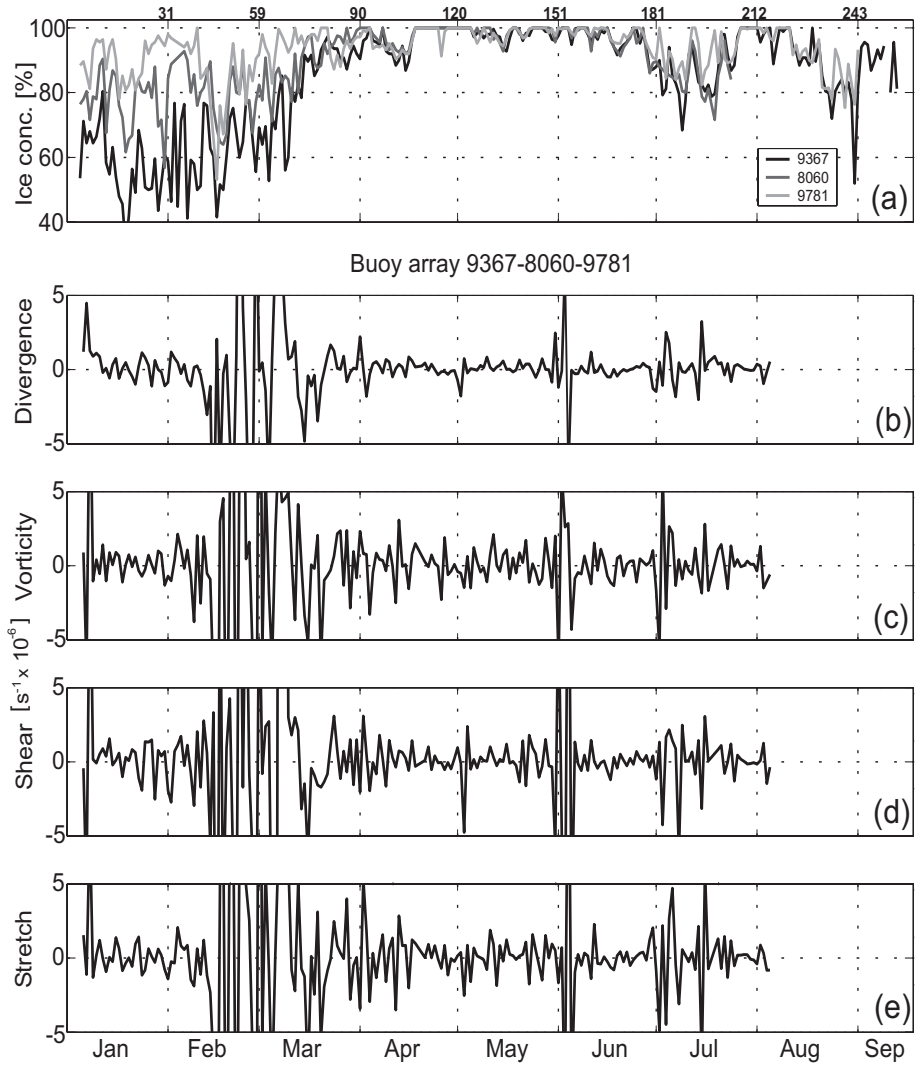

Figure 5. SSMI/AMSR derived sea-ice concentrations at sea-ice (#8060, #9781) and iceberg (# 9367) buoys (a). Associated DKP moments of the sea-ice/iceberg buoy array for days 4 to 216, b) divergence, c) vorticity, d) shear deformation and e) stretch deformation of the ensemble.

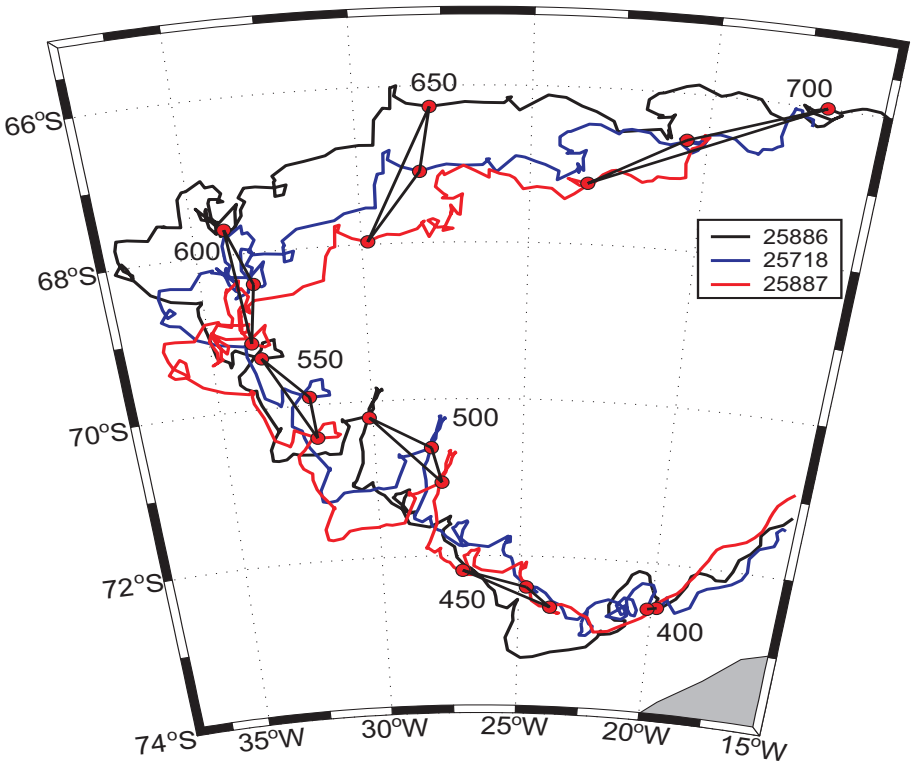

Figure 6. Excerpt of drift trajectories of iceberg buoys # 25886, #25718, and # 25887 released in Dec/00 off Neumayer Station. Array positions every 50 days are overlaid as joined triangles.

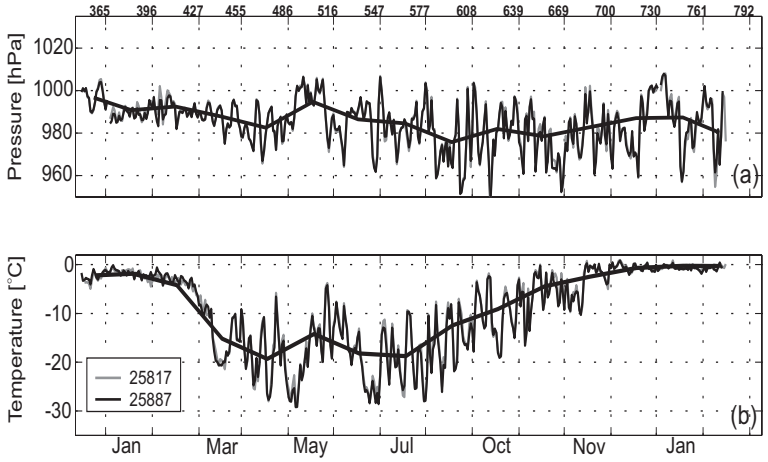

Figure 7. a) ECMWF sea level pressure vs time and b) ECMWF air temperature vs time at iceberg buoys # 25886, #25718, and # 25887 resembling atmospheric conditions during the drift in the eastern Weddell Sea. The solid curve in a and b represents the monthly mean value.

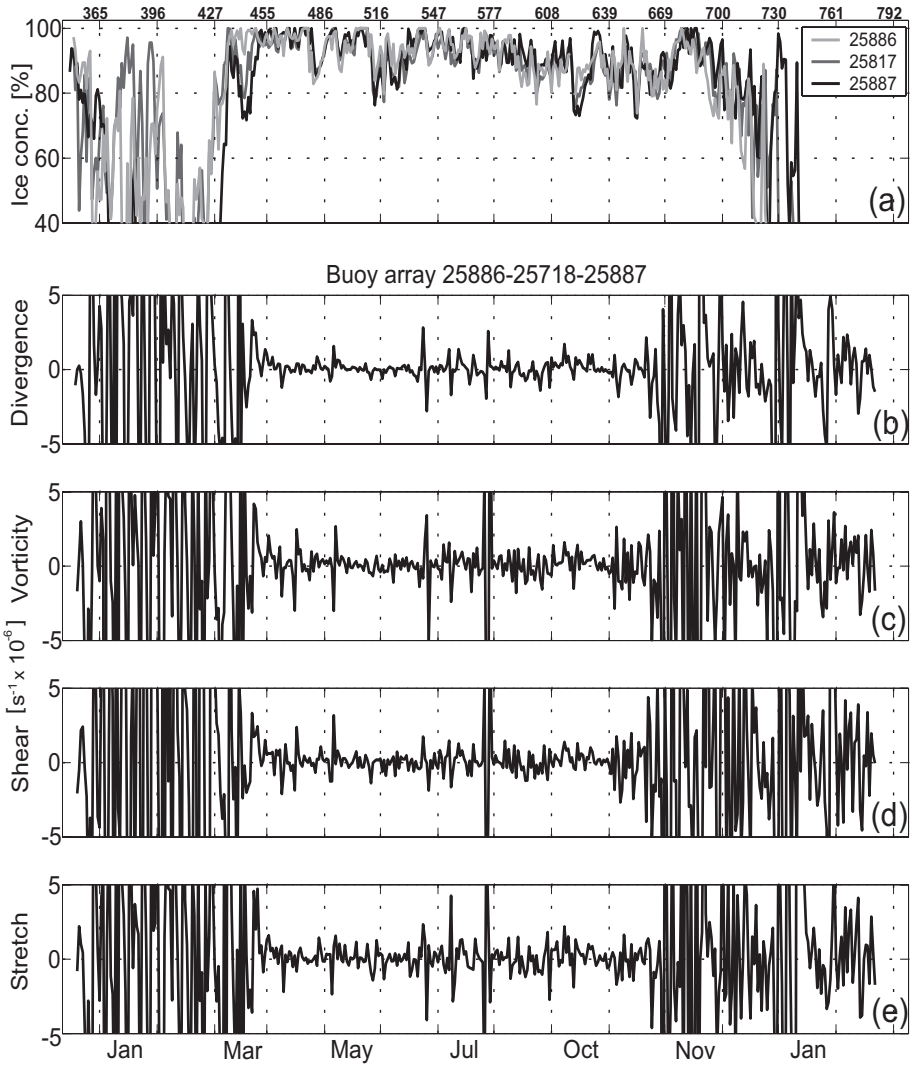

Figure 8. SSMI/AMSR derived sea-ice concentrations for the drift period depicted in Fig. 6 at iceberg (# 25886, #25718, and # 25887) buoys (a). Associated DKP moments of iceberg buoy array for days 349 (2000) to 780 (2002), b) divergence, c) vorticity, d) shear deformation, and e) stretch deformation of the ensemble.

Table 1. Iceberg buoy Information (L: Length, W: Width, F: Freeboard)

No.		ID	Date of Deployment	Iceberg dimension L	W	F [m]	Lat	Lon	Last Date of transmission	Lat	Lon
1		9803	15.01.99	250	250	40	54.752°S	0.353°E	25.03.99	53.746°S	17.955°E
2		9802	15.01.99	1830	530	50	55.617°S	0.927°W	08.02.99	56.146°S	4.845°E
3		9835	16.01.99	740	560	30-40	58.643°S	0.003°E	17.02.99	58.313°S	5.157°E
4		9665	20.01.99	600	300	30	70.375°S	9.482°W	21.12.99	71.233°S	12.400°W
5		9782	23.01.99	650	280	30-40	70.263°S	11.243°W	17.01.01	58.251°S	13.548°W
6		9834	23.01.99	740	280	25-35	70.500°S	11.493°W	07.02.01	58.389°S	0.146°W
7	Jan/99	9667	29.01.99	370	100	15-25	75.120°S	47.162°W	18.02.03	61.270°S	82.730°W
8		9831	30.01.99	520	220	30-50	75.266°S	51.590°W	05.05.00	59.178°S	16.611°W
9		9781	31.01.99	750	350	20-35	75.214°S	53.652°W	25.12.00	57.358°S	34.818°W
10		8069	01.02.99	1200	280	45-60	75.446°S	55.123°W	10.03.02	63.933°S	44.065°W
11		9832	05.02.99	7000	4000	9-65	75.325°S	52.832°W	10.11.99	71.668°S	58.730°W
12		8057	01.03.99	650	370	45	70.364°S	10.226°W	04.03.01	63.903°S	39.421°W
13		14956	18.01.00	380	290	35	69.168°S	4.948°W	18.03.01	61.067°S	1.449°W
14		9803	18.01.00	1100	550	45	69.801°S	4.758°W	30.05.02	62.419°S	30.805°E
15		9835	18.01.00	380	380	45	69.737°S	6.163°W	15.04.01	59.737°S	8.147°W
16		14954	20.01.00	1400	600	65	70.152°S	7.931°W	21.02.01	59.055°S	14.781°W
17		14959	01.02.00	740	350	45	68.401°S	10.828°W	25.02.01	62.067°S	8.395°W
18	Jan/00	14961	01.02.00	1300	600	12	68.573°S	9.633°W	10.06.00	67.082°S	14.240°W
19		9802	07.02.00	480	220	30	69.724°S	22.128°E	25.02.02	62.914°S	1.425°E
20		14958	08.02.00	1100	200	50	69.133°S	16.461°E	02.04.01	60.944°S	16.574°W
21		9372	15.02.00	350	350	50	66.185°S	16.700°E	12.03.00	66.761°S	51.096°E
22		25719	14.12.00	370	180	25	66.283°S	4.490°W	03.02.01	66.514°S	7.147°W
23		25926	14.12.00	180	180	25	66.363°S	4.386°W	07.01.01	66.396°S	6.855°W
24		25649	14.12.00	370	180	20	66.966°S	5.783°W	16.05.01	64.275°S	14.272°W
25		25887	15.12.00	750	370	30	69.666°S	6.435°W	28.02.03	56.505°S	7.487°E
26		25827	15.12.00	1100	750	42	69.752°S	5.776°W	28.02.03	66.905°S	51.221°W
27		25718	16.12.00	400	200	25	70.348°S	7.822°W	27.02.01	56.371°S	6.519°E
28		25886	16.12.00	360	360	36	69.994°S	7.975°W	20.02.02	64.736°S	10.565°W
29	Dec/00	25650	16.12.00	180	180	20	69.983°S	9.425°W	03.03.01	70.990°S	20.118°W
30		14957	19.12.00	360	360	35	69.480°S	5.294°W	31.08.02	61.620°S	28.365°W
31		25826	21.12.00	750	370	12	68.450°S	0.834°W	02.03.01	69.389°S	12.642°W
32		25925	22.12.00	440	180	30	66.904°S	0.186°W	28.03.01	67.451°S	5.986°W
33		8067	12.12.01	550	550	60	69.710°S	6.885°W	20.03.03	63.312°S	27.883°W
34		9366	27.12.01	740	370	45	68.740°S	0.099°E	01.09.02	64.074°S	18.086°W
35		9367	04.01.02	250	50	25	71.005°S	41.878°W	01.09.02	60.215°S	33.355°W
36		9832	07.01.02	1900	500	60	68.961°S	56.182°W	01.09.02	66.418°S	58.534°W
37		9665	07.01.02	15000	2700	70	68.612°S	55.992°W	01.09.02	66.646°S	58.656°W
38		8068	09.01.02	40000	17000	50	68.114°S	55.792°W	12.02.03	51.862°S	38.264°W
39	Jan/02	8057	09.01.02	2900	1440	60	68.009°S	56.623°W	01.09.02	65.697°S	57.967°W
40		8066	10.01.02	8000	8000	60	67.217°S	55.246°W	20.03.03	57.307°S	40.841°W
41		8061	11.01.02	1200	800	60	66.891°S	52.305°W	01.02.03	61.303°S	54.661°W
42		9831	15.01.02	10000	3000	45	66.344°S	54.120°W	01.09.02	59.723°S	50.288°W
43		9360	11.12.02	200	200	26	65.953°S	2.482°W	17.01.03	66.309°S	5.3465°W
44		14959	13.12.02	1600	750	40	70.348°S	8.341°W	05.03.04	67.252°S	51.8125°W
45		14958	13.12.02	380	380	25	70.227°S	7.950°W	05.03.04	65.743°S	37.9341°W
46		14960	14.12.02	380	380	40	70.277°S	9.664°W	06.03.04	64.679°S	29.4136°W
47		14956	16.12.02	380	380	20	69.101°S	0.497°E	07.03.04	64.381°S	23.5693°W
48		8056	18.12.02	180	180	10	66.121°S	0.413°E	17.02.03	66.340°S	2.6913°W
49	Dec/02	14955	19.12.02	180	150	50	64.868°S	0.283°E	22.12.02	64.749°S	0.5078°E
50		9835	23.12.02	200	100	15	64.022°S	8.284°E	10.01.03	64.496°S	7.2639°E
51		14954	29.12.02	1000	300	30	69.183°S	22.534°E	07.03.04	74.971°S	49.7205°W
52		14961	29.12.02	300	300	35	69.401°S	21.578°E	07.03.04	69.835°S	9.4345°E

Table 2. Meander coefficient for iceberg buoys with a drift history of more than 6 months. The drift region is partitioned into the Coastal Current (CC), the inner Weddell Sea (IW) and northern Weddell Sea (NW) areas, where the IW area represents the main northward flow and the NW area the main eastward flow including the Scotia Sea.

ID		CC	IW	NW
8057	Jan/99	1.3	2.8	-
8069		-	2.0	2.1
9781		-	2.4	2.1
9782		1.4	2.3	3.1
9831		-	1.7	1.5
9834		1.9	2.8	2.4
9667		-	1.8	1.7

ID		CC	IW	NW
9802	Jan/00	1.3	2.9	2.7
9803		1.4	3.0	1.9
9835		2.3	3.1	-
14954		1.8	2.5	1.9
14956		1.5	3.3	3.0
14958		1.6	3.0	-
14959		-	3.2	3.2

Table 2. Table 2 continue

ID		CC	IW	NW
8067	Dec/00	1.8	3.7	1.4
9366		1.8	3.0	1.7
9367		-	1.9	1.5
8066		-	2.3	2.5
8068		-	1.8	1.5
9831		-	2.1	2.9
8068		-	1.8	1.5
8060		-	2.2	1.5
9781		-	1.9	1.4
9728		-	1.7	1.1

ID		CC	IW	NW
14957	Jan/02	1.5	4.2	1.9
25718		1.7	3.4[1]	1.9
25827		1.6	1.6[2]	-
25886		1.4	2.1	2.2
25887		1.2	2.7	1.9

Table 2. Table 2 continue

ID		CC	IW	NW
14954	Dec/02	1.3	-	-
14956		1.7	4.9	-
14958		1.5	3.8	-
14959		1.4	-	-
14960		1.3	3.7	-